Online Finger-Knuckle-Print Verification for Personal Authentication

Lin Zhang[a], Lei Zhang[a*], David Zhang[a] and Hailong Zhu[b]

[a] Biometrics Research Center, Department of Computing, The Hong Kong Polytechnic University

[b] Research Institute of Innovative Product & Technology, The Hong Kong Polytechnic University

Abstract. Biometric based personal authentication is an effective method for automatically recognizing, with a high confidence, a person's identity. By observing that the texture pattern produced by bending the finger knuckle is highly distinctive, in this paper we present a new biometric authentication system using finger-knuckle-print (FKP) imaging. A specific data acquisition device is constructed to capture the FKP images, and then an efficient FKP recognition algorithm is presented to process the acquired data in real time. The local convex direction map of the FKP image is extracted, based on which a local coordinate system is established to align the images and a region of interest is cropped for feature extraction. For matching two FKPs, a feature extraction scheme which combines orientation and magnitude information extracted by Gabor filtering is proposed. An FKP database, which consists of 7,920 images from 660 different fingers, is established to verify the efficacy of the proposed system and promising results are obtained. Compared with the other existing finger-back surface based biometric systems, the proposed FKP system achieves much higher recognition rate and it works in real time. It provides a practical solution to finger-back surface based biometric systems and has great potentials for commercial applications.

Keywords: Biometrics, finger-knuckle-print, personal authentication

* Corresponding author. Email: cslzhang@comp.polyu.edu.hk. This research is supported by the Ho Tung Fund under grant no. 5-ZH25 and the Hong Kong Polytechnic University research fund under grant no. G-YH54.

1. Introduction

Personal authentication is a common concern to both industries and academia due to its numerous applications such as physical access control, computer security, banking and law enforcement, etc. Biometrics, which refers to the unique physiological or behavioral characteristics of human beings, can be used to distinguish between individuals and hence can serve as an ideal solution to this problem. With the rapid development of computer techniques, in the past three decades researchers have exhaustively investigated the use of a number of biometric characteristics, including fingerprint [1-3], face [4-5], iris [6-7], retina [8-9], palmprint [10-16], hand geometry [17-19], hand vein [20-21], finger surface [22-27], inner-knuckle-print [28-29], voice [30], ear [31], gait [32] and signature [33-34], etc. Although many biometric techniques are still under the stage of research and development, some biometric systems have been used in a large scale; for example, the Hong Kong government has been using the fingerprint recognition system as the automated passenger clearance system (e-channel) since 2004 [35].

Among various kinds of biometric identifiers, hand-based biometrics has been attracting considerable attention over recent years. Fingerprint [1-3], palmprint [10-16], hand geometry [17-19], hand vein [20-21], and inner-knuckle-print [28-29] have been proposed and well investigated in the literature. The popularity of hand-based biometrics should be attributed to its high user acceptance. In fact, the image pattern in the finger knuckle surface is highly unique and thus can serve as a distinctive biometric identifier. Woodard and Flynn [22-23] are among the first scholars who exploit the use of finger knuckle surface in biometric systems. They set up a 3-D finger back surface database with the Minolta 900/910 sensor. For feature extraction, they used the curvature based shape index to represent the finger back surface. Woodard's work makes a good effort to validate the uniqueness of outer finger surface as a biometric characteristic. However, their work did not provide a practical solution to establishing an efficient system using the outer finger surface features. The cost, size and weight of the Minolta 900/910 sensor limit the use of it in a practical biometric system, and the time-consuming 3-D data acquisition and processing limit its use in real-time applications. In addition, they did not fully exploit the finger knuckle texture information in feature extraction.

Later, Kumar and Ravikanth [24-25] proposed another approach to personal authentication by using

2-D finger-back surface imaging. They developed a system to capture hand-back images and then extracted the finger knuckle areas by some preprocessing steps. The subspace analysis methods such as PCA, LDA and ICA were combined to do feature extraction and matching. With Kumar's design, the acquisition device is doomed to have a large size because nearly the whole hand back area has to be captured, despite the fact that the finger knuckle area only occupies a small portion of the acquired image. Furthermore, subspace analysis methods may be effective for face recognition but they may not be able to effectively extract the distinctive line and junction features from the finger knuckle surface. In Kumar's later work [26-27], they used the robust line orientation code proposed in [16] to extract the orientation of the finger-back surface images.

In this paper, a new hand-based biometric technique, namely finger-knuckle-print (FKP), is developed for online personal authentication. FKP refers to the image pattern of the outer surface around the phalangeal joint of one's finger, which is formed by bending slightly the finger knuckle. A specially designed acquisition device is constructed to collect FKP images. Unlike the systems in [22] and [25] which first capture the image of the whole hand and then extract the finger or finger knuckle surface areas, the proposed system captures the image around the finger knuckle area of a finger directly, which largely simplifies the following preprocessing steps. Meanwhile, with such a design the size of the imaging system can be greatly reduced, which improves much its applicability. Since the finger knuckle will be slightly bent when being imaged in the proposed system, the inherent finger knuckle print patterns can be clearly captured and hence the unique features of FKP can be better exploited.

After an FKP image is captured, a region of interest (ROI) needs to be cropped from the original image for the following feature extraction. An efficient FKP ROI extraction algorithm is proposed based on the intrinsic characteristics of FKP images. For matching two FKP ROI images, we propose a new feature extraction scheme which combines orientation and magnitude information extracted by Gabor filters. Experimental results show that it outperforms the other state-of-the-arts coding based feature extraction methods, such as CompCode [12], OrdinalCode [14], RLOC [16, 26-27] and BOCV [10], in FKP recognition. To evaluate the performance of the proposed technique, an FKP database was established using our prototype system, which consists of 7,920 images from 660 different fingers. Experimental results demonstrated that the proposed FKP based authentication system can verify the personal identity in real

time with a high recognition rate. Compared with the other existing finger knuckle surface based biometric systems [22-25], the proposed one performs much better in terms of both the recognition accuracy and the speed.

The rest of this paper is organized as follows. Section 2 introduces the design and structure of the FKP image acquisition device. Section 3 describes the FKP image preprocessing and the ROI extraction method. Section 4 investigates the FKP feature extraction method and the related matching scheme. Section 5 reports the experimental results. Finally, conclusions are presented in Section 6.

2. The Finger-Knuckle-Print (FKP) Recognition System

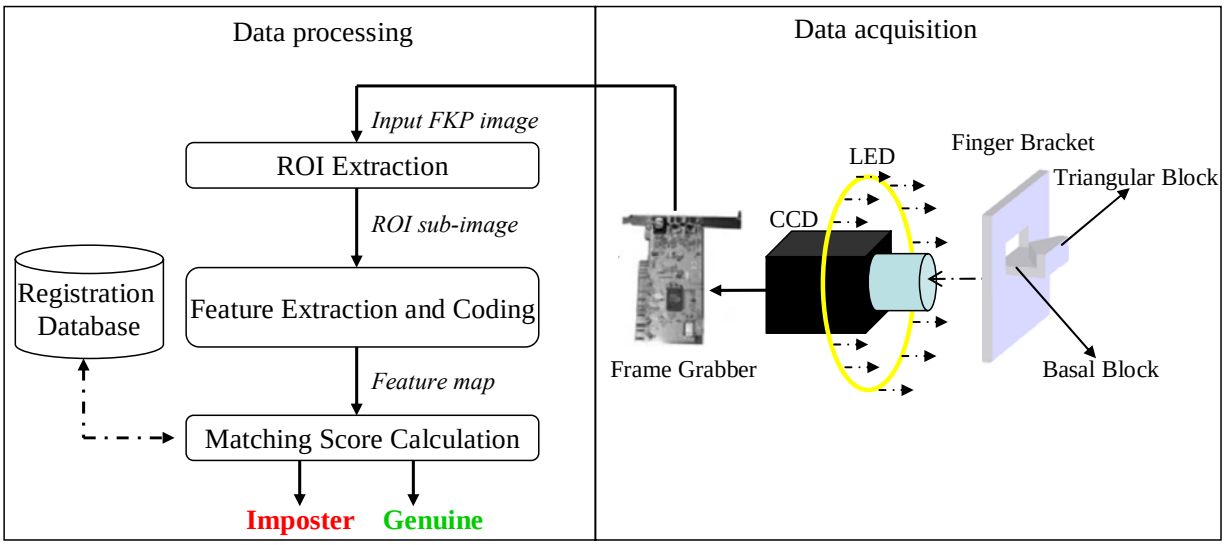

Fig. 1: Structure of the proposed FKP-based personal authentication system. The whole system is composed of a data acquisition module and a data processing module.

The schematic diagram of our FKP based personal authentication system is shown in Fig. 1. The system is composed of a data acquisition module and a data processing module. The data acquisition module is composed of a finger bracket, a ring LED light source, a lens, a CCD camera and a frame grabber. The captured FKP image is inputted to the data processing module, which comprises three basic steps: ROI (region of interest) extraction, feature extraction and coding, and matching. Fig. 2 shows the outlook of our FKP image acquisition device whose overall size is 160mm×125mm×100mm.

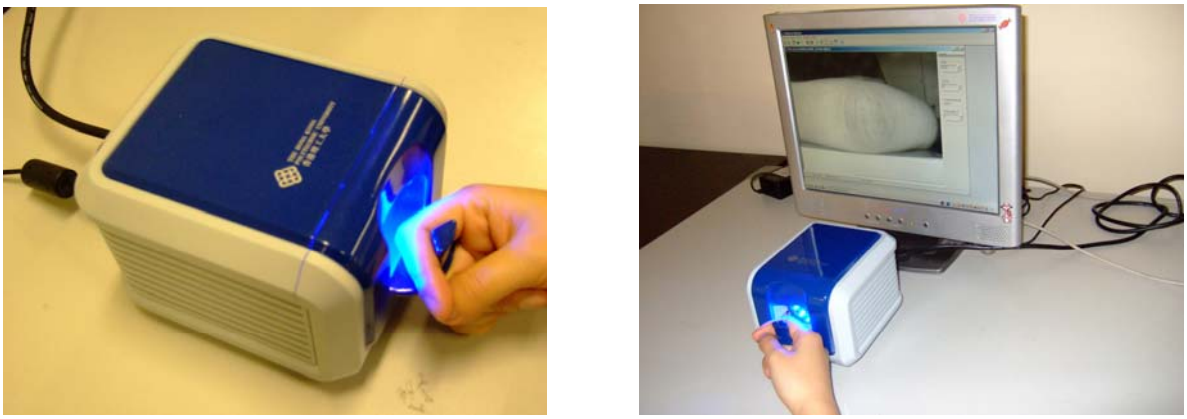

(a) (b)

Fig. 2: (a) The outlook of the developed FKP image acquisition device; (b) The device is being used to collect FKP samples.

A critical issue in data acquisition is to make the data collection environment as stable and consistent as possible so that variations among images collected from the same finger can be reduced to the minimum. In general, a stable image acquisition process can effectively reduce the complexity of the data processing algorithms and improve the image recognition accuracy. Meanwhile, we want to put as little constraint as possible on the users in order for high user friendliness of the system. With the above considerations, a semi-closed data collection environment is designed in our system. The LED light source and the CCD camera are enclosed in a box so that the illumination is nearly constant. One difficult problem is how to make the gesture of the finger be nearly constant so that the captured FKP images from the same finger are consistent. In our system, the finger bracket is designed for this purpose.

Refer to Fig. 1, a basal block and a triangular block are used to fix the position of the finger joint. In data acquisition, the user can easily put his/her finger on the basal block with the middle phalanx and the proximal phalanx touching the two slopes of the triangular block. Such a design aims at reducing the spatial position variations of the finger in different capturing sessions. The triangular block is also used to constrain the angle between the proximal phalanx and the middle phalanx to a certain magnitude so that line features of the finger knuckle surface can be clearly imaged.

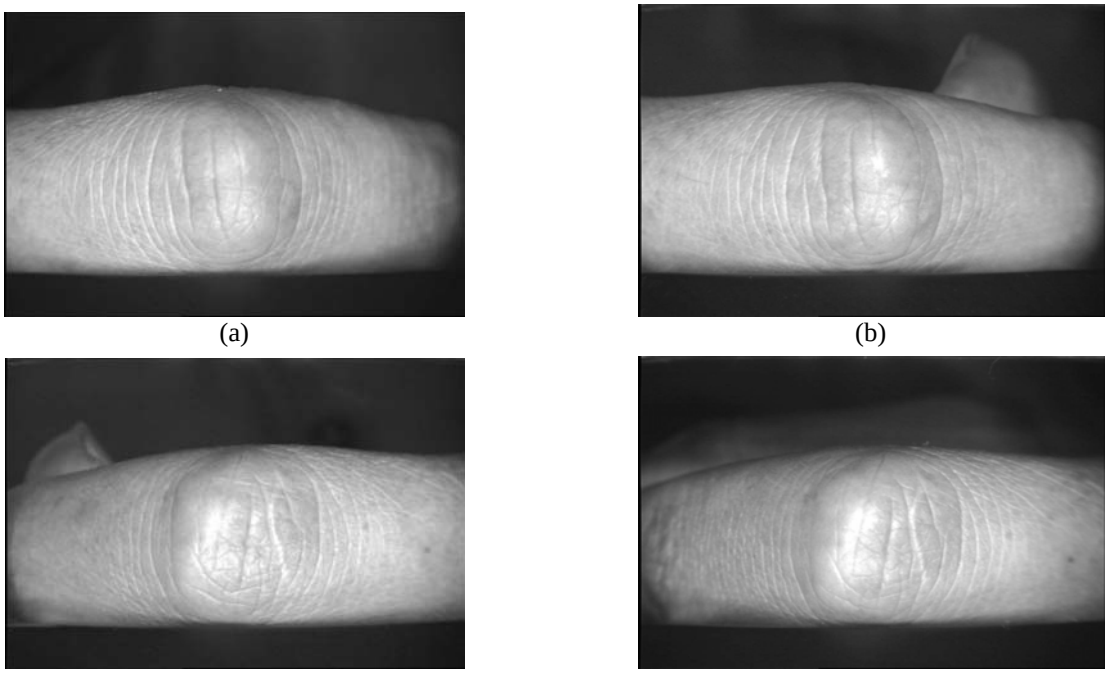

Fig. 3: Sample FKP images acquired by the developed system. (a) and (b) are from one finger while (c) and (d) are from another finger. Images from the same finger are taken at two different sessions with an interval of 56 days.

After the image is captured, it is sent to the data processing module for preprocessing, feature extraction and matching (refer to Sections 3 and 4 for details). The size of the acquired FKP images is 768×576 under a resolution about 400 dpi. Fig. 3 shows four sample images acquired by the developed device. Two images in the first row are from one finger and images in the second row are from another finger. Example images for the same finger were captured at two different collection sessions with an interval of 56 days. We see that by using the developed system, images from the same finger but collected at different times are very similar to each other. Meanwhile, images from different fingers are very different, which implies that FKP has the potential for personal identification.

3. ROI (Region of Interest) Extraction

FKP images collected from different fingers are very different. On the other hand, for the same finger, images collected at different collection sessions will also vary because of the variation of spatial locations of the finger. Therefore, it is necessary and critical to align FKP images by adaptively constructing a local coordinate system for each image. With such a coordinate system, an ROI can be cropped from the original

image in order for reliable feature extraction and matching. In this section, we will propose an algorithm for the local coordinate system determination and ROI sub-image extraction.

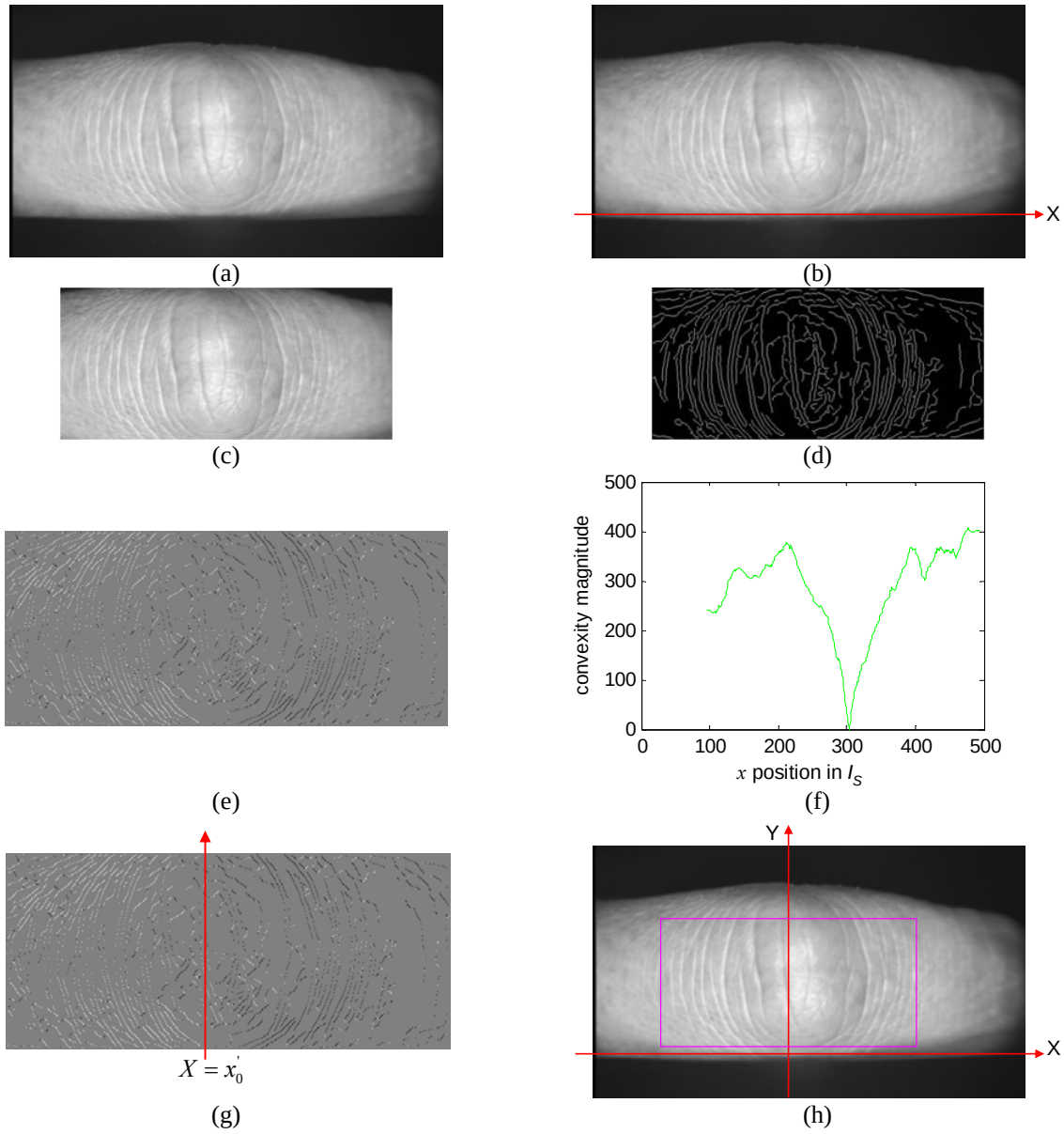

Fig. 4: Illustration for the ROI extraction process. (a) I_D image which is obtained by a down-sampling operation after a Gaussian smoothing; (b) X-axis of the coordinate system, which is the line $Y = Y_0$, fitted from the bottom boundary of the finger; (c) I_S image extracted from I_D; (d) I_E image obtained by applying a Canny edge detector on I_S; (e) I_{CD} image obtained by applying the convex direction coding scheme to I_E; (f) plot of $conMag(x)$ for a typical FKP image; (g) line $X = x_0'$, where $x_0' = \arg\min_x (conMag(x))$; (h) ROI coordinate system, where the rectangle indicates the area of the ROI sub-image that will be extracted.

Because the finger is always put flatly on the basal block when the FKP image is captured, the bottom boundary of the finger is stable in every image and can be taken as the X-axis of the ROI coordinate system.

However, the *Y*-axis is much more difficult to determine. Intuitively, we want to locate the *Y*-axis in the center of the phalangeal joint so that most of the useful features in the FKP image can be preserved within the ROI. It can be observed that line features on the two sides of the phalangeal joint have different convex directions. Taking this fact as a hint, we propose to code line pixels based on their convex directions and then make use of the convex direction codes to determine the *Y*-axis. Fig. 4 illustrates the main steps of the coordinate system determination and the ROI extraction. In the following, we describe these steps in detail.

Step 1: image down-sampling

The size of the captured FKP image is 768×576 under a resolution of 400dpi. Based on our experiments, it is not necessary to use such a high resolution for feature extraction and matching. Therefore, we apply a Gaussian smoothing operation to the original image, and then down-sample the smoothed image to about 150 dpi (see Section 5.2 for the discussion of resolution selection). The down-sampling operation has two advantages. First it can significantly reduce the computational cost by reducing the data amount. Second, the Gaussian smoothing will suppress the noise in the original image, which can benefit the following feature extraction and matching steps. We denote by I_D the down-sampled image and Fig. 4-a shows such an image.

Step 2: determine the *X*-axis of the coordinate system

Refer to Fig. 4-b, the bottom boundary of the finger can be easily extracted by a Canny edge detector. Actually, this bottom boundary is nearly consistent to all FKP images because all the fingers are put flatly on the basal block in data acquisition. By fitting this boundary as a straight line, the *X*-axis of the local coordinate system is determined.

Step 3: crop a sub-image I_S from I_D

Useful information which can be used for personal identification only resides in a portion of the whole FKP image. Therefore, we first crop a sub-image I_S from the original image for the convenience of later processing. The left and right boundaries of I_S are two fixed values evaluated empirically. The top and bottom boundaries are estimated according to the boundary of real fingers. Fig. 4-c shows an example I_S

image. This roughly cropped sub-image will be used to calculate the *Y*-axis so that an accurate ROI image can be cropped.

Step 4: Canny edge detection

By applying Canny edge detector to I_S, the corresponding edge map I_E can be obtained. See Fig. 4-d for an example.

Step 5: convex direction coding for I_E

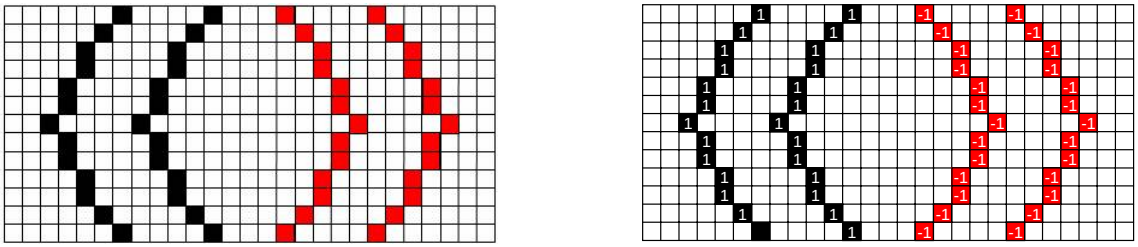

(a) (b)

Fig. 5: (a) Ideal model for FKP "curves"; (b) Convex direction coding scheme.

Based on the local convexity characteristics of the edge map I_E, we can code I_E to get the convex direction coding map I_{CD}. At this step, each pixel on I_E will be given a code to represent the local convex direction of this pixel. The underlying principle of this coding scheme is as follows. Based on the observation of FKP images, we abstract an ideal model for "curves" on an FKP image as shown in Fig. 5-a. In this model, an FKP "curve" is either convex leftward or convex rightward. We code the pixels on convex leftward curves as "1", the pixels on convex rightward curves as "-1", and the other pixels not on any curves as "0". Fig. 5-b illustrates the coding scheme. In our system, we regard the edges obtained in step 4 as "curves" and this convex direction coding is performed on I_E. The pseudo code of this algorithm is given in Table 1:

Table 1. ***Algorithm Convex_Direction_Coding (I_E)***

Input: I_E ($m \times n$ binary edge map computed in step 4)
Output: I_{CD} ($m \times n$ convex direction code map)

Begin module

$y_{mid} = \frac{height\ of\ I_E}{2}$;
for each $I_E(i, j)$ **do**
  if $I_E(i, j) = 0$ // *it is a background pixel*
    $I_{CD}(i, j) = 0$;
  else if $I_E(i+1, j-1) = 1$ *and* $I_E(i+1, j+1) = 1$ // *it is a bifurcation pixel*
    $I_{CD}(i, j) = 0$;
  else if $(I_E(i+1, j-1) = 1$ *and* $i <= y_{mid})$ *or* $(I_E(i+1, j+1) = 1$ *and* $i > y_{mid})$
    $I_{CD}(i, j) = 1$;
  else if $(I_E(i+1, j+1) = 1$ *and* $i <= y_{mid})$ *or* $(I_E(i+1, j-1) = 1$ *and* $i > y_{mid})$
    $I_{CD}(i, j) = -1$;
  end if
end for

End module

After convex direction coding, each I_{CD} point is assigned a value 0, 1 or -1. Fig. 4-e shows an I_{CD} map in false color image format. White pixels on it are the ones with convexity value "1"; black pixels are the ones with value "-1"; and gray pixels are of value "0".

Step 6: determine the *Y*-axis of the coordinate system

Consider the ideal FKP curve model set up at step 5. For an FKP image, "curves" on the left part of phalangeal joint are mostly convex leftward and those on the right part are mostly convex rightward. Meanwhile, "curves" in a small area around the phalangeal joint do not have obvious convex directions. Based on this observation, at a horizontal position x (x represents the column) of an FKP image, we define the "convexity magnitude" as:

$$conMag(x) = abs\left(\sum_{W} I_{CD}\right) \tag{1}$$

where W is a window that is symmetrical about the axis $X = x$ and W is of size $d \times h$ with h being the height of I_S. d is experimentally chosen as 35 in this paper. The "convexity magnitude" is proposed to measure how strong the dominant convex direction is in a local area on the FKP image. The characteristic of the FKP image suggests that $conMag(x)$ will reach a minimum around the center of the phalangeal joint and this position can be used to set the Y-axis of the coordinate system. Let

$$x_0' = \arg\min_{x}\left(conMag(x)\right) \tag{2}$$

Then $X = x_0'$ can be set as the Y-axis. Fig. 4-f plots the curve $conMag(x)$ of an FKP image and Fig. 4-g

shows the vertical line $X = x_0'$, which is the *Y*-axis of the ROI system.

Step 7: crop the ROI image

Now that we have fixed the *X*-axis and *Y*-axis, the local coordinate system can then be determined. Refer to Fig. 4-h, with the constructed coordinate system, the ROI sub-image I_{ROI} can be extracted from I_D with a fixed size, which is empirically set as 110×220 in our system.

Fig. 6 shows some examples of the extracted ROI images. We can see that the proposed coordinate system construction and ROI extraction method can effectively align the different FKP images and normalize the area for feature extraction. Such operations reduce greatly the variations caused by the various poses of the finger in data collection.

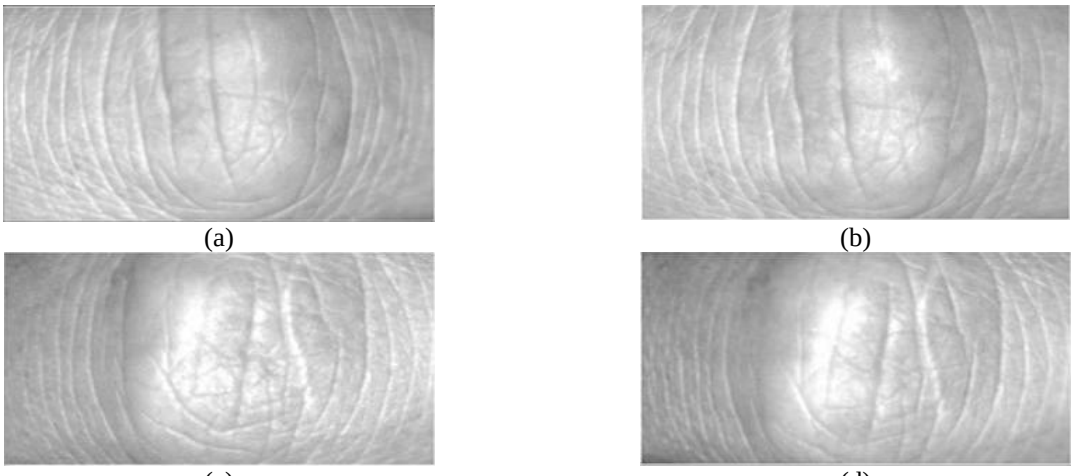

Fig. 6: Sample ROI images extracted by the proposed method. These four images are ROI images for the sample images shown in Fig. 3, respectively.

4. FKP Feature Extraction and Matching

The Gabor filtering technique can simultaneously extract the spatial-frequency information from the original signal [36]. Since 1980s, it has been widely used as an effective tool to fulfill the feature extraction job in face, iris, fingerprint and palmprint systems. In [37], Loris and Alessandra described a Gabor feature selection technique. The Gabor filter can produce three types of features – magnitude, phase, and

orientation, which can be used separately or jointly in different systems [38]. In this paper, we propose a method combining the orientation and magnitude features for FKP recognition. Experimental results in Section 5 verifies that the proposed scheme performs better in FKP recognition than the other coding-based methods, such as BOCV [10], CompCode [12], OrdinalCode [14] and RLOC [16, 26-27].

The Gabor function has several slightly different forms in the literature and here we adopt the one proposed by Lee [39]:

$$G(x, y, \omega, \theta) = \frac{\omega}{\sqrt{2\pi}\kappa} e^{-\frac{\omega^2}{8\kappa^2}(4x'^2 + y'^2)} \left(e^{i\omega x'} - e^{-\frac{\kappa^2}{2}} \right) \tag{3}$$

where $x' = (x-x_0)\cos\theta + (y-y_0)\sin\theta$, $y' = -(x-x_0)\sin\theta + (y-y_0)\cos\theta$, $(x_0, y_0)$is the center of the function, ω is the radial frequency in radians per unit length and θ is the orientation of the Gabor functions in radians. κ is defined by $\kappa = \sqrt{2\ln 2}\left(\frac{2^{\delta}+1}{2^{\delta}-1}\right)$, where δ is the half-amplitude bandwidth of the frequency response. ω can be determined by $\omega = \kappa / \sigma$, where σ is the standard deviation of the Gaussian envelop.

Using Gabor filtering, next we propose an improved competitive coding (ImCompCode) method to exploit the orientation information, and then we propose a magnitude coding (MagCode) method to exploit magnitude information. Finally, we fuse these two kinds of features in FKP matching.

4.1. Improved competitive coding (ImCompCode) for orientation feature extraction

At each pixel $I_{ROI}(x,y)$, we extract the orientation information and represent it as an "orientation code". This process is similar to the CompCode scheme in [12].

With a bank of Gabor filters, the orientation feature at each pixel $I_{ROI}(x,y)$ can be extracted. In our system, we only use the real part of the Gabor filter to perform this job. Mathematically, this orientation coding process can be represented as:

$$oriCode(x, y) = \arg\min_{j} \left\{ I_{ROI}(x, y) * G_R(x, y, \theta_j) \right\} \tag{4}$$

where symbol * represents the convolution operation, G_R represents the real part of the Gabor function G, $\theta_j = j\pi / J, j = \{0,\ldots, J - 1\}$, and J represents the number of different orientations.

Here we improve the original CompCode scheme. Often on an FKP image, there are some pixels lying on relatively "plane" areas, i.e. these pixels do not reside on any lines and consequently do not have a dominate orientation. Accordingly, the J Gabor filter responses at such pixels do not have much variation. If we still assign an orientation code to it, this code may not be stable and will be sensitive to noise, making the performance of feature representation and matching decreased. Therefore, those "plane" pixels should be removed from orientation coding. We define the "orientation magnitude" at a pixel as:

$$oriMag(x, y) = \frac{abs\left(\max(R) - \min(R)\right)}{\max\left(abs\left(\max(R)\right), abs\left(\min(R)\right)\right)} \tag{5}$$

where $R = \{R_j = I_{ROI}(x, y) * G_R(x, y, \theta_j)\}$, $j = \{0,\ldots, J - 1\}$ are the Gabor filtering responses at this pixel. The "orientation magnitude" $oriMag(x, y)$ can measure how likely the pixel (x, y) has a dominant orientation. If it is smaller than a threshold, we reckon that this pixel has no dominant orientation and the corresponding competitive code is assigned as J.

Based on our experimental results, using 6 Gabor filters of different orientations is enough. This is in accordance with the conclusion made by Lee in [39] that the simple neural cells are sensitive to specific orientations with approximate bandwidths of $\pi / 6$. Thus, we choose 6 orientations, $\theta_j = j\pi / 6, j = \{0,\ldots, 5\}$ for the competition. The pseudo code for our ImCompCode scheme is summarized in Table 2 and Fig. 7 (a)~(d) are ImCompCode maps for FKP ROI images shown in Fig. 6.

Table 2. ***Algorithm ImCompCode (I_{ROI})***

Input: I_{ROI} ($m \times n$ ROI sub-image)
Output: $ImCompCode$ ($m \times n$ integer matrix)

Begin module
for each $I_{ROI}(x, y)$ **do**
$R = \left\{R_j = I_{ROI}(x, y) * G_R(x, y, \theta_j)\right\}$, where $\theta_j = j\pi / 6, j = \{0,1,...5\}$
$oriMag = \frac{abs\left(\max(R) - \min(R)\right)}{\max\left(abs\left(\max(R)\right), abs\left(\min(R)\right)\right)}$
if $oriMag < T$ *// this pixel does not have a dominant orientation*
$ImCompCode(x, y) = 6$;
else
$ImCompCode(x, y) = \arg\min_j \left\{R_j\right\}$
end if
end for
End module

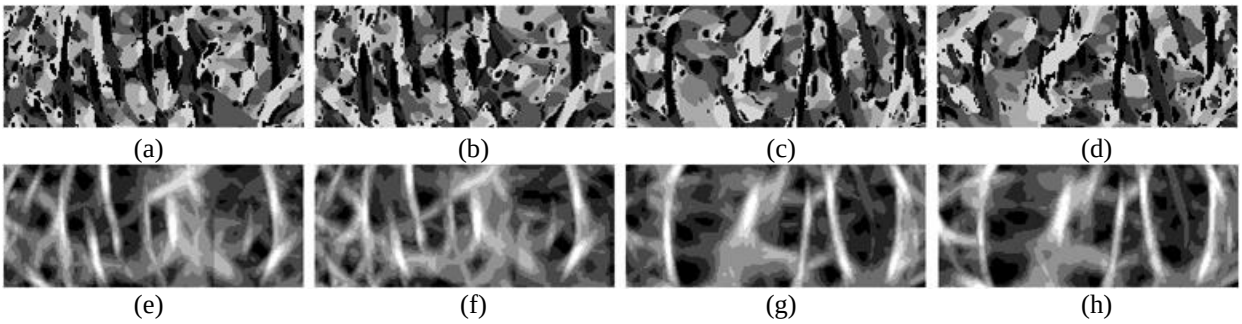

Fig. 7: (a) ~ (d) and (e) ~ (h) are ImCompCode maps and MagCode maps for the FKP ROI images shown in Fig. 6, respectively.

4.2. Magnitude coding (MagCode) for magnitude feature extraction

Besides orientation information, we also want to exploit magnitude information from Gabor filter responses. The magnitude of the Gabor filter response at $I_{ROI}(x, y)$ is:

$$\sqrt{\left(I_{ROI}(x,y) * G_R(x,y,\omega,\theta_j)\right)^2 + \left(I_{ROI}(x,y) * G_I(x,y,\omega,\theta_j)\right)^2} \tag{6}$$

where G_R and G_I represent the real part and the imaginary part of the Gabor function G respectively. However, in order to reduce the computational cost, when generating the magnitude code map, we want to make use of the temporary results generated from the "orientation coding" process. Thus, we still only use the real part of the Gabor filter and define the magnitude at $I_{ROI}(x, y)$ as:

$$mag(x,y) = \max_j \left(abs\left(I_{ROI}(x,y) * G_R(x,y,\theta_j)\right)\right) \tag{7}$$

Then a localized quantization is applied to $mag(x, y)$ to get the magnitude code. This process can be expressed as:

$$magCode(x,y) = ceil\left(\left(mag(x,y) - lmin\right) \Big/ \left(\frac{lmax - lmin}{N}\right)\right) \tag{8}$$

where N is the number of quantization levels, $lmin = \min_{(x,y)\in W_m} \left(mag(x,y)\right)$, and $lmax = \max_{(x,y)\in W_m} \left(mag(x,y)\right)$. W_m is a $w \times w$ window centered at (x, y). The resulting magnitude code is an integer within 1~ N. w and N can be tuned by experiments on a sub-dataset and they are experimentally set as 31 and 8 in this paper, respectively. Fig. 7 (e) ~ (h) show magnitude code maps for FKP ROI images presented in Fig. 6.

4.3. FKP matching

Suppose we are comparing two FKP ROI images, P and Q. Let P_o and Q_o be the two orientation code maps; and let P_m and Q_m be the two magnitude code maps. At first, we will calculate the matching distance between P_o and Q_o and the matching distance between P_m and Q_m respectively, and then fuse the two matching distances together as the final matching distance between P and Q.

When calculating the matching distance between P_o and Q_o, we adopt the angular distance proposed in [12], which is defined as:

$$angD(P,Q) = \frac{\sum_{y=1}^{Rows}\sum_{x=1}^{Cols} G\left(P_o(x,y), Q_o(x,y)\right)}{(J/2)\cdot S} \tag{9}$$

where S is the area of the code map, and

$$G\left(P_o(x,y), Q_o(x,y)\right) = \begin{cases} 1, P_o(x,y) = 6 \; and \; Q_o(x,y) \neq 6 \\ 1, P_o(x,y) \neq 6 \; and \; Q_o(x,y) = 6 \\ 0, P_o(x,y) = Q_o(x,y) \\ \min\left(P_o(x,y) - Q_o(x,y), Q_o(x,y) - \left(P_o(x,y) - 6\right)\right), if \; P_o(x,y) > Q_o(x,y) \; and \; P_o(x,y) \neq 6 \\ \min\left(Q_o(x,y) - P_o(x,y), P_o(x,y) - \left(Q_o(x,y) - 6\right)\right), if \; P_o(x,y) < Q_o(x,y) \; and \; Q_o(x,y) \neq 6 \end{cases} \tag{10}$$

The matching distance between P_m and Q_m is defined as:

$$magD(P,Q) = \frac{\sum_{y=1}^{Rows}\sum_{x=1}^{Cols} abs\left(P_m(x,y) - Q_m(x,y)\right)}{(N-1)\cdot S} \tag{11}$$

Then, the final matching distance between P and Q can be fused from *angD* and *magD* as:

$$dist(P,Q) = (1-\lambda)\cdot angD(P,Q) + \lambda \cdot magD(P,Q) \tag{12}$$

where λ is used to control the contribution of *magD* to *dist* and it is experimentally set as 0.15 in our system.

Taking into account the possible translations in the extracted ROI sub-image (with respect to the one extracted in the enrolment), multiple matches are performed by translating one set of features in horizontal and vertical directions. And in such case, S is the area of the overlapping parts of the two code maps. The minimum of the resulting matching distances is considered to be the final distance. The ranges of the horizontal translation and the vertical translation are empirically set as -8 to 8 and -4 to 4 in this paper, respectively.

5. Experimental Results

5.1. Database establishment

In order to evaluate the proposed FKP-based personal authentication system, a database was established using the developed FKP image acquisition device (refer to Fig.1 and Fig. 2). FKP images were collected from 165 volunteers, including 125 males and 40 females. Among them, 143 subjects were 20~30 years old and the others were 30~50 years old. The database will be available in the website of Biometrics Research Center, The Hong Kong Polytechnic University (http://www.comp.polyu.edu.hk/~biometrics/).

We collected samples in two separate sessions. In each session, the subject was asked to provide 6 images for each of the left index finger, the left middle finger, the right index finger and the right middle finger. Therefore, 48 images from 4 fingers were collected from each subject. In total, the database contains 7,920 images from 660 different fingers. The average time interval between the first and the second sessions was about 25 days. The maximum and minimum time intervals were 96 days and 14 days respectively. In all of the following experiments, we took images collected at the first session as the gallery set and images collected at the second session as the probe set. To obtain statistical results, each test image in the probe set was matched with all the training images in the gallery set. If the test image and the training image were from the same finger, the matching between them was counted as a genuine matching; otherwise it was counted as an imposter matching.

5.2. Selection of the image resolution

The resolution of original FKP images acquired in our system is about 400 dpi, which may not be optimal in terms of the accuracy and efficiency of FKP verification. In fact, many factors, such as the storage space, the computational cost, the employed feature extraction and matching method, and the recognition accuracy, should be considered in selecting a suitable resolution of the FKP images for a more efficient biometric system. To this end, we conducted a series of experiments to select the “optimal” resolution and set the selection criterion as: the minimum resolution with which a satisfying verification performance could be

obtained. The experiments were performed on a sub-dataset of the whole FKP database. In this sub-dataset, there were 120 classes, including 1,440 images. With respect to the feature extraction method, the CompCode was used [12]. We smoothed the original images by using a Gaussian kernel and then down-sampled the images to five lower resolutions: 200 dpi, 170 dpi, 150 dpi, 120 dpi and 100 dpi. The experimental results are summarized in Table 3.

Table 3. EERs obtained under different resolutions

resolution	EER (%)
200 dpi	1.73
170 dpi	1.41
150 dpi	1.36
120 dpi	1.71
100 dpi	1.92

Based on the results listed in Table 3, it can be seen that 150 dpi is a good choice. It leads to the lowest EER, while the resolution is much smaller than the original one (400 dpi). This will reduce the computational cost and speed up the feature extraction and matching processes significantly. Therefore, in all of the following experiments, we used the FKP images with a resolution 150 dpi.

5.3. FKP verification

Verification aims to answer the question of “whether the person is the one he/she claims to be”. In order to show and explain the performance of the proposed system clearly, 3 experiments were conducted. In each experiment, we evaluated and compared the performance of five coding based feature extraction methods: CompCode [12], OrdinalCode [14], RLOC [16], BOCV [10] and the proposed ImCompCode&MagCode. The CompCode has been introduced in Section 4.1. In OrdinalCode, differences between Gaussians from two orthogonal directions were used to extract the orientation fields. The scales of the 2D Gaussian function along two orthogonal directions in OrdinalCode were set as 2.2 and 5.5 in our implementation. The RLOC method is based on the modified finite Radon transform. It was originally proposed for palmprint recognition [16], and was later adopted for feature extraction of the finger-back -surface images [26-27]. In our implementation of RLOC, the “line width” was set as 2 and the kernel size was 14×14. BOCV [10] is a

recently proposed method for palmprint recognition which tends to represent multiple orientations for a local region. The threshold for the binarization used in BOCV was set as 0 in this paper. Gabor filters used in CompCode, BOCV and the proposed ImCompCode&MagCode were all of the form (3), and the parameters were set as: $\delta = 3.3$ and $\sigma = 5.3$.

5.2.1. Experiment 1. In the first experiment, all classes of FKPs were involved. Each image in the probe set was matched against all the images in the gallery set. Therefore, in this experiment there were 660 (165×4) classes and 3,960 (660×6) images in the gallery set and the probe set each. The numbers of genuine matchings and imposter matchings are 23,760 and 15,657,840, respectively. By adjusting the matching threshold, a ROC (Receiver Operating Characteristic) curve, which is a plot of Genuine Accept Rate (GAR) against False Accept Rate (FAR) for all possible thresholds, can be created. The ROC curve can reflect the overall performance of a biometric system. Fig. 8-a shows ROC curves generated by the five different FKP recognition schemes and Table 4 lists the corresponding EERs, from which we can see that the proposed ImCompCode&MagCode scheme performs the best among the five methods evaluated in terms of EER. Distance distributions of genuine matchings and imposter matchings obtained by the proposed scheme are plotted in Fig. 8-b.

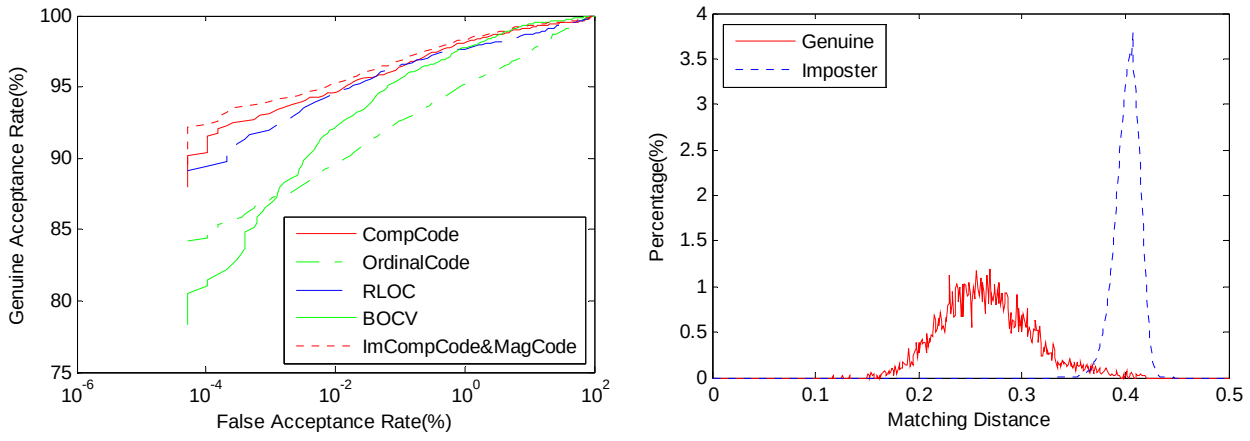

(a) (b)

Fig. 8: (a) ROC curves obtained by the five recognition methods in experiment 1. (b) Distance distributions of genuine matchings and imposter matchings with the proposed scheme in experiment 1.

Table 4. EERs obtained by different methods in experiment 1

Method	EER (%)
CompCode	1.72
OrdinalCode	3.83
RLOC	1.93
BOCV	1.82
ImCompCode&MagCode	1.48

5.2.2. Experiment 2. As mentioned in Section 5.1, our database contains FKPs from four types of fingers, left index fingers, left middle fingers, right index fingers and right middle fingers. The aim of this experiment is to evaluate the performance of the proposed FKP-based personal authentication system on each type of fingers separately. For each type of FKPs, the gallery and the probe each contains 165 classes and 990 (165×6) sample images, and the numbers of genuine matchings and imposter matchings are 5,940 and 974,160 respectively. Similarly, five FKP recognition schemes were evaluated. ROC curves for different finger types and by different recognition schemes are shown in Fig. 9. Experimental results in terms of EER are summarized in Table 5 for comparison.

The experimental results indicate that in general the right middle and index fingers perform better than their left counterparts in terms of EER. This is probably because that the majority of people who provided FKP samples in our database are right-handed. They would feel more convenience to use our image acquisition device with their right hand than with the left one, which consequently leads to a result that the variations of finger poses of right hand fingers are less severe than left hand fingers. Remarkable variations of finger poses would cause severe affine transforms and deformations between two FKP images of the same finger, which lead to more challenge to FKP recognition.

Table 5. EERs (%) by different schemes in experiment 2

finger type	CompCode	OrdinalCode	RLOC	BOCV	ImCompCode&Magcode
left index	2.06	2.69	2.20	2.45	1.73
left middle	1.96	4.07	2.27	2.42	1.78
right index	1.82	3.66	2.07	2.43	1.44
right middle	1.87	4.15	2.32	2.30	1.64

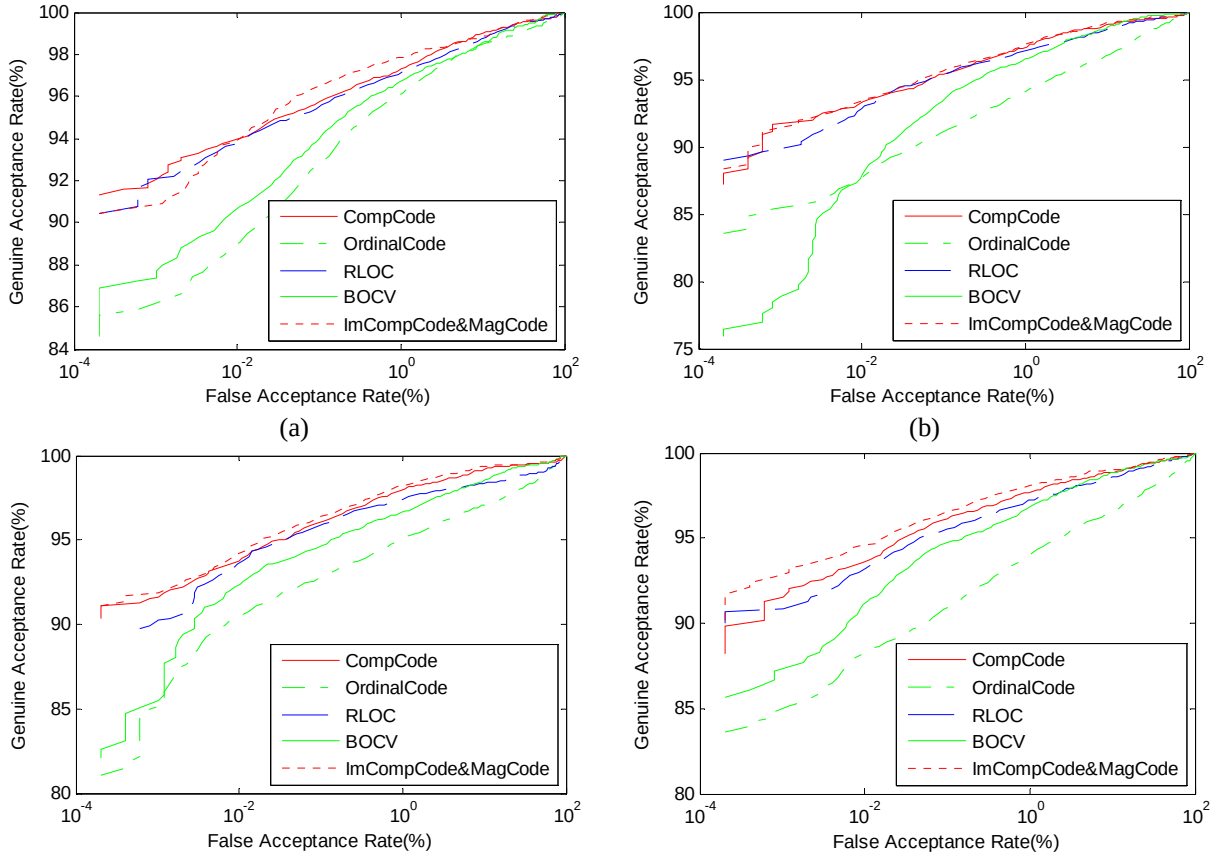

Fig.9: ROC curves for FKPs from (a) left index fingers, (b) left middle fingers, (c) right index fingers, and (d) right middle fingers.

5.2.3. Experiment 3. The goal of this experiment is to investigate the system's performance when we fuse information from 2 or more fingers of a person. In fact, in such a case the system works as a kind of multi-modal system with a single biometric trait but multiple units [40]. Suppose that we want to fuse information from the right index FKP and the right middle FKP. Each template in the enrolment database will be composed by a right index FKP t_{ri} and a right middle FKP t_{rm}. When matching, a client's right index FKP c_{ri} and right middle FKP c_{rm} will be matched to t_{ri} and t_{rm} respectively to get two matching distances, d_{ri} and d_{rm}. Then d_{ri} and d_{rm} will be fused according to some fusion rules to obtain the final matching distance, by which the client's identity can be identified.

With respect to fusion rules, in this paper we simply examined the SUM rule and the MIN rule as they are easily to be implemented and can well reflect the system's performance. The SUM rule is defined as:

$$d_{sum} = \sum d_i \tag{13}$$

and the MIN rule is defined as:

$$d_{min} = min(d_i) \tag{14}$$

where d_i is the matching distance of the client's i^{th} finger.

We tested several different fusion schemes of fingers with the two fusion rules. Results are presented in Table 6, from which it can be easily observed that by integrating information from more fingers the recognition performance of the system could be largely improved. We can also find that the SUM rule works better than the MIN rule in our system.

Table 6. EERs (%) obtained in experiment 3

fingers in fusion	CompCode		OrdinalCode		RLOC		BOCV		ImCompCode &MagCode	
	S-rule	M-rule	S-rule	M-rule	S-rule	M-rule	S-rule	M-rule	S-rule	M-rule
left index left middle	0.33	0.67	0.64	0.72	0.26	0.68	0.41	0.45	**0.20**	0.63
right index right middle	0.32	0.39	0.71	0.79	0.34	0.37	0.36	0.47	**0.26**	0.36
left index right index	0.36	0.67	0.84	0.76	0.42	0.91	0.63	0.63	**0.26**	0.64
left middle right middle	0.29	0.33	0.90	0.87	0.33	0.30	0.43	0.42	**0.27**	0.30
All the four	0	0.03	0.02	0.05	0	0.16	0.01	0.09	**0**	0.02

5.4. Speed

The FKP recognition software is implemented using Visual C#.Net 2005 on a Dell Inspiron 530s PC embedded Intel E6550 processor and 2GB of RAM. Computation time for the key processes are listed in Table 7. The execution time for data preprocessing and ROI extraction is 198ms. The time for ImCompCode&MagCode-based feature extraction and matching is 105ms and 1.6ms, respectively. Thus, the total execution time for one verification operation is less than 0.5s in our prototype system, which is fast enough for real-time applications. We believe that with the optimization of the implementation, the system's efficiency could be much further improved.

Table 7. Computation time for key processes

Method	Time (msec)
ROI extraction	198
Feature extraction	105
Matching	1.6

5.5. Discussion

FKP is a new member in the biometrics family compared with other biometric identifiers. As mentioned in the section of Introduction, Woodard and Flynn [22-23] did some salient work to validate the uniqueness of features from finger-back surfaces by using 3D imaging, and Kumar [24-25] integrated 2D finger knuckle surface information with the finger shape information in their system. However, such a system is doomed to have a relatively large size because they need to collect the image of the whole hand. Complex preprocessing steps are also needed to extract the finger knuckle area which only occupies a small portion of the whole acquired image. In our system, we make use of a triangular block to control the finger freedom. This gadget does not sacrifice the user convenience and it is easy to use. Such a design brings the following merits: 1) the acquisition device could be easily made to a small size; 2) image around the finger knuckle area is captured directly, which largely simplifies the following data preprocessing steps; and 3) since the finger knuckle is slightly bent when being captured, the distinctive FKP texture patterns can be clearly imaged, which makes the proposed FKP system have high accuracy.

Advantages of the proposed system could be reflected by experimental results on FKP verification. For comparison, experimental results in [22] and [25] are extracted from the original papers and listed in Table 8 and partial experimental results by our system are also presented. The scale of the dataset used in our experiment is much larger than the ones mentioned in [22] and [25]. Woodard's result [22] and Kumar's result [25] were obtained by fusing information from three and four fingers, respectively. It can be clearly seen that the proposed system performs much better even if we incorporate information from fewer fingers. Particularly, if four fingers are used, our system could achieve an EER of 0.

Table 8. Comparison of experimental results

method	gallery classes	gallery samples	probe classes	probe samples	Finger types for fusion	EER (%)
[22]	132	660	177	531	r-index, r-middle, r-ring	5.5
[25]	105	420	105	210	index, middle, ring, little	1.39
Ours	165	990	165	990	r-index, r-middle	0.26
Ours	165	990	165	990	r-index, r-middle, l-index, l-middle	0

It should be noted that although we use a triangular block to control the finger freedom in FKP image acquisition, there are still variations for the same finger at different collection sessions. Sometimes such variations can result in severe affine transforms or even non-elastic deformations among intra-class FKPs. And as a result, feature maps of such FKPs can have large matching distances. Fig. 10 shows a typical example. The two FKP images in Fig. 10 are from the same finger but are recognized as different classes in our system. In fact, high intra-class matching distances (higher than 0.41) are mainly resulted from such kind of geometric deformations. For example, in experiment 1, all the 43 genuine matchings with matching distances higher than 0.41 could be attributed to such cases. Hence, how to reduce the effects of affine transforms and deformations will be a direction of our future work.

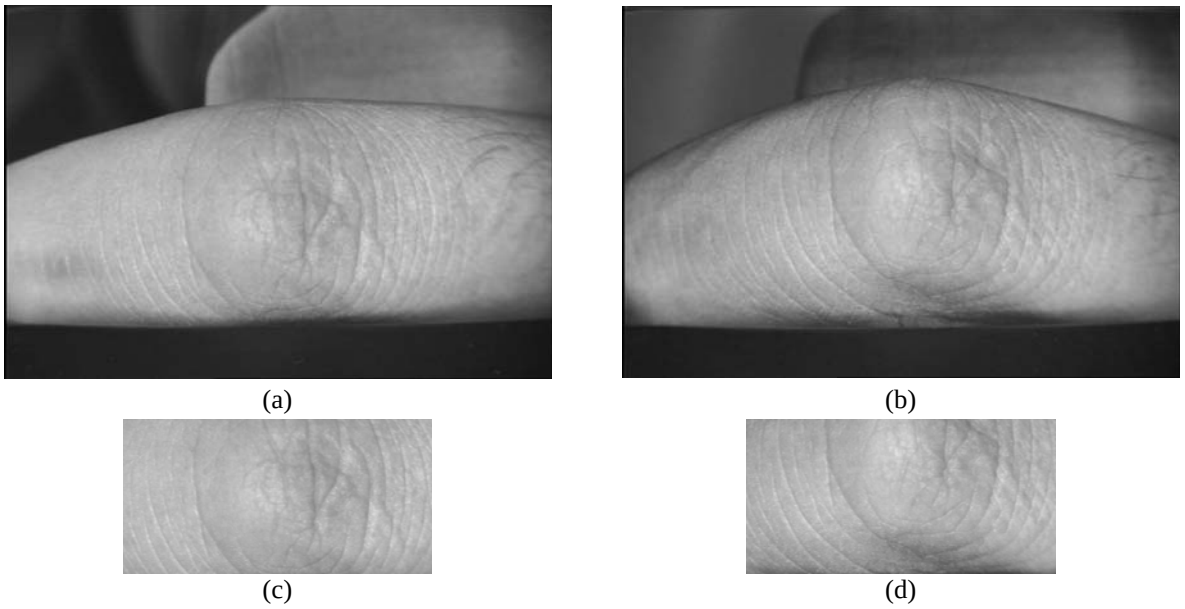

Fig. 10: (a) and (b) are two intra-class FKP images captured by our system. (c) and (d) are their ROI sub-images. There is an obvious pose variation between the two FKPs and they are recognized as different classes in our system.

6. Conclusions

This paper presents a new approach to online personal authentication using finger-knuckle-print (FKP), which has distinctive line features. A cost-effective FKP system, including a novel image acquisition device and the associated data processing algorithms, is developed. A region of interest (ROI) extraction algorithm is proposed to align and extract the FKP sub-image for feature extraction. For efficient FKP matching, a

feature extraction scheme is proposed to exploit both orientation and magnitude information extracted by Gabor filters. To evaluate the performance of the proposed system, an FKP database is established, consisting of 7,920 images from 660 different fingers. Extensive experiments are conducted and promising results demonstrate the efficiency and effectiveness of the proposed technique. Compared with other existing finger back surface based systems, the proposed one has merits of high accuracy, high speed, small size and cost-effective. It has a great potential to be future improved and employed in real commercial applications. In the future, we will focus on how to deal with affine or even non-elastic deformations between FKP images from the same finger to further improve the system's performance.

References

[1] A.K. Jain, P. Flynn, A. Ross, Handbook of Biometrics, Springer, 2007.

[2] D. Maltoni, D. Maio, A.K. Jain, S. Prabhakar, Handbook of Fingerprint Recognition, Springer, 2003.

[3] N. Ratha, R. Bolle, Automatic Fingerprint Recognition Systems, Springer, 2004.

[4] K. Delac, M. Grgic, Face Recognition, I-Tech Education and Publishing, 2007.

[5] H. Wechsler, Reliable Face Recognition Methods - System Design, Implementation and Evaluation, Springer, 2006.

[6] J. Daugman, High confidence visual recognition of persons by a test of statistical independence, IEEE Trans. Pattern Analysis and Machine Intelligence 15 (11) (1993) 1148-1161.

[7] J. Daugman, How iris recognition works, IEEE Trans. Circuits and Systems for Video Technology 14 (1) (2004) 21-30.

[8] R. B. Hill, Retinal identification, in Biometrics: Personal Identification in Networked Society, A. Jain, R. Bolle, and S. Pankati, Eds., Kluwer Academic, 1999.

[9] H. Borgen, P. Bours, S.D. Wolthusen, Visible-Spectrum Biometric Retina Recognition, in: Proceedings of the International Conference on Intelligent Information Hiding and Multimedia Signal Processing, 2008, pp. 1056-1062.

[10] Z.H. Guo, D. Zhang, L. Zhang, W.M. Zuo, Palmprint verification using binary orientation co-occurrence vector, Pattern Recognition Letters 30 (13) (2009) 1219-1227.

[11] D. Zhang, W. K. Kong, J. You, M. Wong, Online palmprint identification, IEEE Trans. Pattern Analysis and

Machine Intelligence 25 (9) (2003) 1041-1050.

[12] W. K. Kong, D. Zhang, Competitive coding scheme for palmprint verification, in: Proceedings of the ICPR'04, 2004, pp. 520-523.

[13] A. Kong, D. Zhang, M. Kamel, Palmprint identification using feature-level fusion, Pattern Recognition 39 (3) (2006) 478-487.

[14] Z.N. Sun, T.N. Tan, Y.H. Wang, S.Z. Li, Ordinal palmprint representation for personal identification, in: Proceedings of CVPR'05, 2005, pp. 279-284.

[15] D.S. Huang, W. Jia, D. Zhang, Palmprint verification based on principal lines, Pattern Recognition 41 (4) (2008) 1316-1328.

[16] W. Jia, D.S. Huang, D. Zhang, Palmprint verification based on robust line orientation code, Pattern Recognition 41 (5) (2008) 1504-1513.

[17] A.K. Jain, A. Ross, S. Pankanti, A prototype hand geometry-based verification system, in: Proceedings of the 2nd International Conference on Audio- and Video-based Biometric Person Authentication, 1999, pp. 166–171.

[18] R. Sanchez-Reillo, C. Sanchez-Avila, A. Gonzalez-Marcos, Biometric identification through hand geometry measurements, IEEE Trans. Pattern Analysis and Machine Intelligence 22 (10) (2000) 1168-1171.

[19] A.K. Jain, N. Duta, Deformable matching of hand shapes for verification, in: Proceedings of ICIP'99, 1999, pp. 857–861.

[20] J.G. Wang, W.Y. Yau, A. Suwandy, E. Sung, Personal recognition by fusing palmprint and palm vein images based on "Lapacianpalm" representation, Pattern Recognition 41 (5) (2008) 1531-1544.

[21] A. Kumar, K.V. Prathyusha, Personal authentication using hand vein triangulation, in: Proceedings of SPIE Biometric Technology for Human Identification, vol. 6944, 2008, pp. 69440E-69440E-13.

[22] D.L. Woodard, P.J. Flynn, Finger surface as a biometric identifier, Computer Vision and Image Understanding 100 (3) (2005) 357–384.

[23] D.L. Woodard, P.J. Flynn, Personal identification utilizing finger surface features, in: Proceedings of CVPR'05, vol. 2, 2005, pp. 1030-1036.

[24] C. Ravikanth, A. Kumar, Biometric authentication using finger-back surface, in: Proceedings of CVPR'07, 2007, pp. 1-6.

[25] A. Kumar, C. Ravikanth, Personal authentication using finger knuckle surface, IEEE Trans. Information Forensics and Security 4 (1) (2009) 98-109.

[26] A. Kumar, Y. Zhou, Human identification using knucklecodes, in: Proceedings of BTAS'09, 2009.

[27] A. Kumar, Y. Zhou, Personal identification using finger knuckle orientation features, Electronic Letters 45 (20) (2009) 1023-1025.

[28] Q. Li, Z. Qiu, D. Sun, J. Wu, Personal identification using knuckleprint, in: Proceedings of SinoBiometrics, 2004, pp. 680-689.

[29] L. Nanni, A. Lumini, A multi-matcher system based on knuckle-based features, Neural Computing & Applications 18 (1) (2009) 87-91.

[30] H. Hollien, Forensic voice identification, Academic Press, 2002.

[31] M. Burge, W. Burger, Ear biometrics, in: Biometrics:Personal Identification in Networked Society, A.K. Jain, R.Bolle, S. Pankanti, Eds., pp. 273-286, Kluwer Academic, 1999.

[32] M.S. Nixon, T.N. Tan, R. Chellappa, Human Identification Based on Gait, Springer, 2006.

[33] R. Plamondona and G. Loretteb, Automatic signature verification and writer identification — the state of the art, Pattern Recognition 22 (2) (1989) 107-131.

[34] C.N. Liu, N.M. Herbst, N.J. Anthony, Automatic signature verification: system description and field test results, IEEE Trans. Systems, Man and Cybernetics 9 (1) (1979) 35-38.

[35] E-channel System of the Hong Kong government, http://www.immd.gov.hk/ehtml/20041216.htm

[36] D. Gabor, Theory of communication, Journal of the Institute of Electrical Engineers 93 (1946) 429-457.

[37] L. Nanni, A. Lumini, On selecting Gabor features for biometric authentication, International Journal of Computer Applications in Technology 35 (1) (2009) 23-28.

[38] A. Kong, An evaluation of Gabor orientation as a feature for face recognition, in: Proceedings of ICPR'08, 2008.

[39] T.S. Lee, Image representation using 2D Gabor wavelet, IEEE Trans. Pattern Analysis and Machine Intelligence 18 (10) (1996) 957-971.

[40] A. Ross, A.K. Jain, Multimodal biometrics: an overview, in: Proceedings of the 12th European Signal Processing Conference, 2004, pp. 1221-1224.